MEMS integration in microfluidics for biosensing applications: static cantilever sensor for DNA detection

Pedro Manuel Lourenço Brito
Engineering Physics

April 2017

1. Introduction

The present situation in health care demands for new devices capable of a faster detection of lower concentrations of a certain biomarker. Hence, a sooner diagnosis can be established and an appropriate treatment can be performed. For this purpose, a biosensor is the key to detect any biomarker or other type of biological material that may help in this process. Actually, not only health care would benefit from the development of improved biosensors, but also fields like process control in industry, environmental monitoring, genetics, biology and drug screening among others [1-5].

An important aspect from the point of view of the industry is the production costs involved. The emergence of microfabrication was decisive for this sector to embrace mass production of micromachined sensors. Although the fabrication processes and materials used in microtechnology are expensive, the final cost of a single device can be very low due to the possibility of batch processing and miniaturization. Different approaches for thin film silicon MEMS fabrication can be employed. However, it is worth to refer the common strategy used at INESC-MN by means of radiofrequency plasma-enhanced chemical vapor deposition (RF-PECVD) of amorphous silicon [6, 7]. This deposition procedure is already optimized for MEMS applications due to previous studies on the parameters and conditions of deposition [8, 9]. Using this process, different stuctures such as cantilevers, bridges and plate resonators have been already studied in the past [10-12]. When designed for biosensing, these structures are functionalized with a proper molecule which transduces the signal resulting from molecular recognition into a well defined mechanical behaviour such as bending or resonance frequency's shift [5, 25, 26, 29-31]. With an appropriate apparatus, it is possible to translate the variations in the mechanical status of these structures into an electrical signal [17-21]. An additional advantage is the possibility of integration with existing components such as CMOS technology given that the fabrication process and specifications are compatible.

The combination of MEMS with a system capable of handling the fluids necessary for biosensing allows the creation of a device with low consumption of biological material to be analysed and potentially a shorter detection time and higher sensitivity also. Microfluidics is the sector of microtechnology that deals with this problem of fluid handling. By using a net of microchannels, pumps, valves and other types of structures it is able to guide, mix, separate or incubate a certain fluid in a microchip [22-24]. The major concern that is currently creating some constraints to this integration is the damping effect that a fluidic medium can have in a mechanical structure under vibration. Furthermore, the incorporation of electrical circuits in a wet environment is a difficult task that can cause malfunctioning in the electrical components.

In the end, a system that is capable to join both MEMS and microfluidics [25-27] would benefit from the advantages of each technology and even allow multiplexing, turning it into a high-throughput sensor for label-free detection [1-4] with a high sensitivity and response rate.

Given the potentialities of MEMS and microfluids, the aim of this thesis is to design and fabricate a device that combines both technologies efficiently. The versatility that MEMS fabrication allow in terms of geometry, materials and dimensions need to be properly analysed so that the purpose of biosensing is conveniently adressed. The chosen MEMS structure is a cantilever working in the static

operation mode. Such structure is easily bendable and its performance is not affected by fluidic damping effects if working in the static mode. The challenge here is to design a robust and reliable structure, maximizing its sensitivity when a surface stress is applied, while aimimg for a multiplexed device with multiple sensors. Microfluidic structures should also be properly designed without compromising the integrity and reliability of the MEMS.

As a second objective, there is the necessity of defining a reactive layer in the structure that is able to recognize a certain molecule in a liquid medium. The target molecule is a specific single strand DNA (ssDNA) that needs to be selectivelly captured by an appropriate probe which is functionalized into the cantilever's surface.

Finally, using the existent systems for MEMS readout, one should be able to characterize the final structures in terms of performance, sensitivity, reliability and robustness. Apart from the measurements in vacuum or air, the behaviour of the system in a liquid medium is also intended to be studied.

2. Theoretical background

A cantilever is a type of MEMS characterized by a beam anchored at one end while the opposite one is free to move as depicted in Figure 1. Since it is able to deflect and oscillate, it is commonly categorized as a microressonator system. As any oscillatory system, cantilevers can be described using a spring-mass model. In fact, when a force is applied on the cantilever's surface, it will bend and its vertical deflection is proportional to the magnitude of the force as stated by Hooke's law.

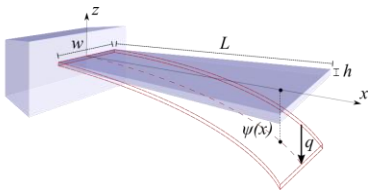

Fig. 1 Schematics of a cantilever.

The spring constant defines the sensitivity of the cantilever since it is a measure of its stiffness. Furthermore, the spring constant of a rectangular cantilever is known to be dependent on the materials used and the geometry established:

$$k = \frac{3EI}{L^3} \quad (1)$$

with E being the Young's modulus of the material used and I the moment of inertia given as function of the dimensions:

$$I = \frac{wh^3}{12} \quad (2)$$

where w, h and L being the width, thickness and length of the cantilever, respectively. By analizing the variables in both equations, it is possible to state that larger aspect ratios in respect to the length will contribute for a larger sensitivity.

The most commonly used operation mode, also called surface stress mode, is the **static** one (Figure 2). In this case, a variation in the surroundings or directly on top of the cantilever's surface creates a surface stress that causes the beam to bend in that region. In biosensing applications, this effect is caused by the adsorption of molecules onto the surface of the cantilever which reduces the surface free energy of its lattice structure. For example, if one intends to measure the relative concentration of a specific highly charged molecule in a medium, it is possible to target that molecule with an appropriate probe and due to the electrostatic interactions between the targets, a different stress will arise on the surface of the cantilever.

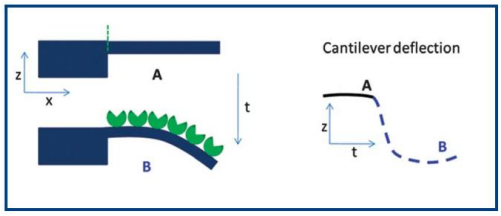

Fig. 2 Cantilever operating in the static mode [3]. In this case, the monitored parameter is the tip deflection.

Stoney's formula for isotropic materials expresses this relation between differential surface stress and the vertical deflection of the tip of the cantilever, ψ_{max}:

$$\Delta\sigma = \frac{Eh^2}{3(1-\nu)L^2}\psi_{max} \quad (3)$$

with ν representing the Poisson's ratio and $\Delta\sigma$ expressing the difference in surface stress between the top and bottom surfaces of the cantilever. In fact, if both surfaces are under the same stress, the deformations will cancel and no deflection will occur. However, for an asymmetrical surface stress, the cantilevered structure will bend either up or

downwards depending on the sign of the differential stress. For example, if the cantilever bends upwards, it is because the stress is tensile, otherwise it is called compressive.

The deflection of the cantilever can be described using the equation of Euler-Bernoulli for a general beam under the effect of an applied load, q:

$$\frac{d^2}{dx^2}\left(EI\frac{d^2\psi}{dx^2}\right) = q \tag{4}$$

where $\psi(x)$ is the function of the curve representing the deflection in z at a certain point x. In a symmetrical and uniform rectangular cantilever the product EI (flexural rigidity) is constant. The final equations for the deflection and slope of the cantilever can be evaluated for the free end ($x = 0$) which is the position that shows the highest values:

$$\psi_{max} = -\frac{qL^4}{8EI} \tag{5}$$

By knowing the deflection at the tip of the cantilever, it is possible to substitute its result in Stoney's formula and find the value of applied surface stress.

Instead of tracking the deflection when a constant load is applied, it is also possible to use the cantilevers actuated in such a way that it induces an oscillation – **dynamic** mode – as suggested in Figure 3. For this reason, cantilevers are also included in the class of microresonators. In a simplified system, without external and damping forces, the oscillation has a natural frequency, ω_{nat}, which is given in terms of the elastic constant, k, and mass, m, of the structure:

$$\omega_{nat} = \sqrt{\frac{k}{m}} \tag{6}$$

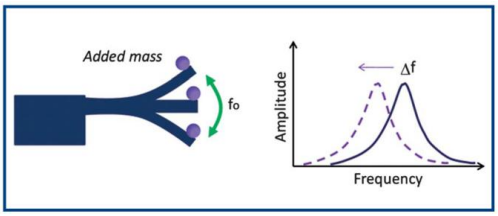

Fig. 3 Cantilever operating in the dynamic mode [3]. Mass is measured by shifts in the resonance frequency.

Nonetheless, since viscous forces have such a strong effect at this scale, it is necessary to include the damping and external forces (for actuation). In such conditions, the motion is described by the differential equation of a typical damped harmonic oscillator. Using the full equation of Euler-Bernoulli, now with dependence in time and assuming a thin rectangular beam with a uniform distribution of mass, one may deduce the frequency of vibration for each mode, f_n:

$$f_n = \frac{k_n^2}{2\pi L^2}\sqrt{\frac{EI}{\rho A}} \tag{7}$$

Another parameter that is possible to determine and represented in Figure 4 is the quality factor, Q:

$$Q = 2\pi\frac{Average\ energy\ stored}{Energy\ lost\ during\ operation} \tag{8}$$

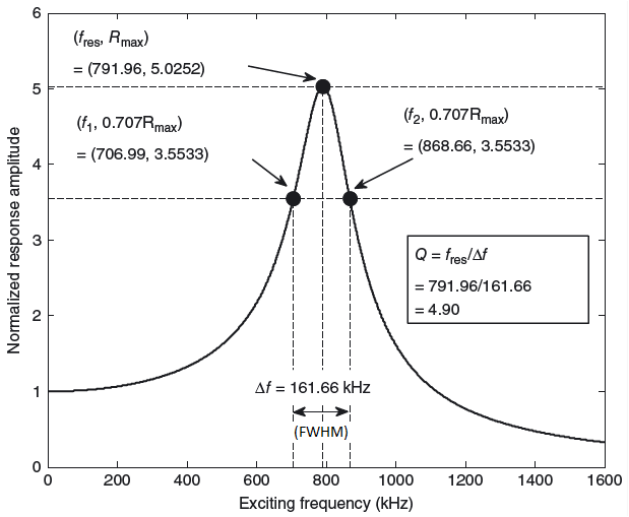

Fig. 4 Example of a resonance peak of a cantilever with the calculation of the Q factor [40].

In a frequency spectrum, this parameter is determined by the "broadening" of the resonance peak since it expresses the relative amount of energy dissipation that is occuring. An experimental method called "-3dB bandwidth method" is commonly used to estimate the Q factor as function of the full width at half maximum (FWHM) of the resonance peak in the spectrum [33, 43].

Since this mode usually operates through electrostatic actuation it is included a pair of parallel electrodes in its design. For this reason, the cantilever is also usually described as an RLC electrical circuit [45, 46], similar to the one schematized in Figure 5. For such configuration and considering small deflections of the beam, the total capacitance of the cantilever can be defined as:

$$C(z) = \frac{\varepsilon_r\varepsilon_0 Lw}{g - z(t)} \tag{9}$$

where $C(z)$ is the static capacitance of the structure, g is the gap distance between the structure and the substrate, ε_r is the relative permittivity of the medium, ε_0 is the permittivity in vacuum and $z(t)$ is the position of the tip.

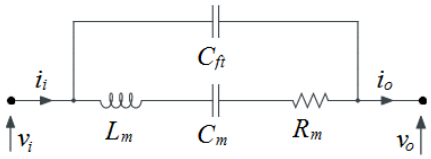

Fig. 5 Butterworth-van-Dyke model for a resonator with parasitic capacitance. C_{ft} is the feed-through capacitance while L_m, C_m and R_m are the electrical equivalents of the mechanical model.

One of the fundamental problems of MEMS is the occurrence of **stiction**. This is the phenomenon related with the effect of adhesion forces on suspended structures and they can be divided in two categories: release stiction and in-use stiction. The first one occurs during the last step of MEMS fabrication in which a sacrificial layer is dissolved (wet etch) using a liquid chemical compound. The other one occurs when operating the MEMS and it is specially critical when using electrostatic actuation. The effect is characterized by the collapsing of the suspended structure when adhesion is sufficiently strong, leading in most of the cases to a permanent adhesion to the substrate, as shown in Figure 6. Commonly, stiction is originated due to capillary, electrostatic, hydrogen bonding and van der Waals forces which gain a strong intensity at microscale. As a matter of fact, a comprehensive physical analysis of the problem of capillary forces acting on microstructures was examined by Mastrangelo and Hsu [50, 51].

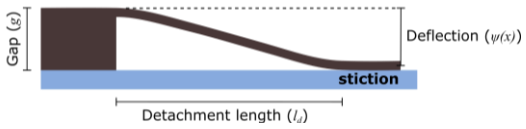

Fig. 6 Cantilever under stiction effect [13]. The beam is permanently stuck to the substrate.

A popular method used for quantifying stiction is the work of adhesion study [13-15]. To perform it, an array of cantilevers is fabricated with different dimensions and after release, it is measured the detachment length, l_d , which is defined by the length of the beam not attached to the substrate and the work of adhesion, W_a , can be calculated:

$$W_a = \frac{3}{8}\frac{Eh^2t^3}{l_d^4} \quad (10)$$

With this value it is possible to predict wether if a structure with specific dimensions is going to suffer stiction.

Microfluidics structures are characterized by a much larger surface-area-to-volume ratio than in a macroscale system. It is known that fluids in microscale are dominated by interactions with the surface, namelly viscous interactions [53, 54]. These are responsible for the different type of flow commonly observed in this regime – parabolic laminar flow (Figure 7). In opposition to the turbulent flow, laminar flow is characterized by an organized flow of particles from the fluid that maintain their velocity and relative positions to neighboring particles. Although laminar flow prevents mixing of two different parallel flows, the reduced dimensions of the channels allow a faster diffusion. According to the Stokes-Einstein formalism for diffusion in fluids, the diffusion rate is proportional to the second power of the diffusion length which for the microscale is very small, validating the previous statement.

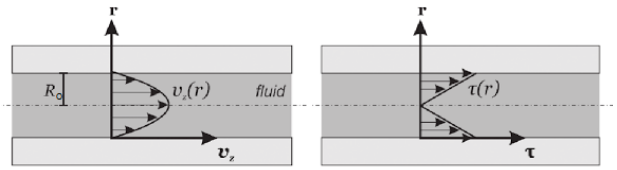

Fig. 7 Schematic of a laminar flow with a parabolic profile due to shear stress felt near the borders of the channel [54].

Another important concept that should be addressed is the surface tension. This quantity results from the tendency of a certain fluid to contract its interface surface in order to reduce its free energy. When considering a certain liquid, the surface tension is the balance between the cohesive forces and the adhesive ones. The cohesive forces between the internal molecules of the liquid cause a contraction of the its surface, while adhesive forces between the molecules from the liquid and the ones from the external fluid cause an expansion of the same surface. When releasing a certain MEMS, it is beneficial to use a liquid (or gas) with a reduced surface tension since the forces pulling the structure towards the substrate become less strong [16].

As widely known, the deoxyribonucleic acid (DNA) is a macromolecule present in the living organisms which carries the genetic information and that can be a biomarker for the early detection of certain diseases [55]. It is

composed by two coiled strands forming a double helix structure. Each strand is composed by many monomers called nucleotides which consist of a phosphate group, a sugar (deoxyribose) and one of the four nucleobases - cytosine (C), guanine (G), adenine (A) or thymine (T). The nucleobases follow a specific order when pairing by means of hydrogen bonding: A binds with T and C with G. This way it is ensured a large specificity for DNA base-pairing, also called hybridization. The two ends of a strand are not identical, since one of them corresponds to a 3' hydroxyl group, while the other is the 5' phosphate group termination. When pairing strands, they are oriented in opposite directions, so that for the same end of the dsDNA, the terminations are not the same. Hybridization is a sensitive process that may exhibit different staibility when subjected to changes in temperature, monomers ratio, strand length, salt concentration and pH.

3. Experimental methods

Biological assays

The process of creating a layer of chemical compounds on top of the cantilever that is able to interact with a specific target molecule is called functionalization. Since the device is operating in the static mode, it is important to ensure a strong interaction between the captured molecules. Apart from that, DNA is also capable of producing tunable self assembled monolayers (SAM's) in terms of density, turning it into a promising candidate as analyte for surface functionalization. The strategy is to immobilize a ssDNA probe into the cantilever's surface by attaching a thiol group to the molecule [30]. Thiol groups are known to have a strong affinity to gold (Au), so by covering the top surface of the cantilever with this material, it is possible to form a SAM of ssDNA. Then, the complementary strand is introduced in the medium and binds to the immobilized probe, creating a surface stress due to electrostatic interactions with neighboring molecules.

The first biological assays are intended to be performed with both fluorescence and chemiluminescence. For that reason, different labels are used to perform the detection of the oligonucleotides. Figure 8 presents a

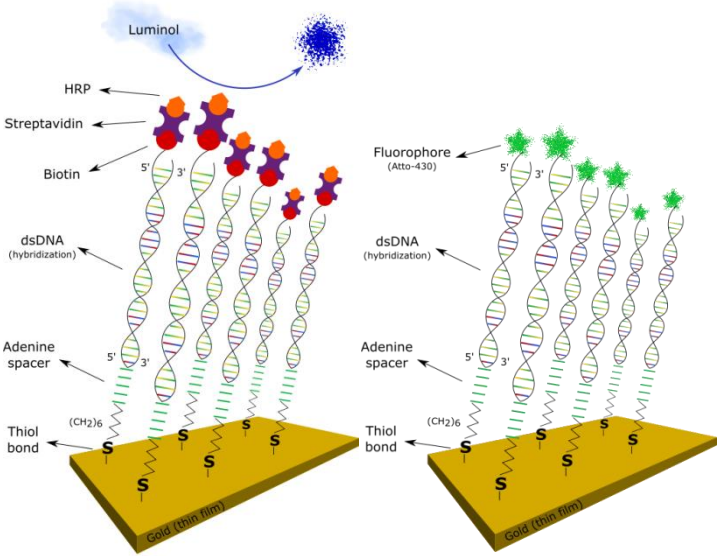

Fig. 8 Schematics of the two techniques employed for target detection: (*left*) chemiluminescence and (*right*) fluorescence.

schematic of the different configurations that were implemented for target detection. For fluorescence microscopy it is just necessary to have a fluorophore attached to the thiolated ssDNA. Chemiluminescence detection requires in this case a more complex procedure: the thiolated ssDNA is attached to a molecule of Biotin which shows a very strong affinity to Streptavidin (Strept); for the detection itself it is used horseradish peroxidase (HRP) which can be conjugated with Strept.

Milli-Q water is used in the preparation of TE 1 M NaCl solution (10 mM Tris-HCl, 1 mM EDTA, 1 M NaCl) which is going to be renamed as TE NaCl for the sake of simplicity. Phosphate buffered saline (PBS) stock solution of 10 mM with pH 7.4 is prepared in 200 mL of deionized (DI) water. Both PBS and TE NaCl are filtered through a 0.2 µm syringe filter from Whatman GmbH and they are subsequently used for preparation of various solutions.

Two types of blocking agents were evaluated during this work: Bovine Serum Albumin (BSA) and Sodium Polyacrilate (PAA). A blocking agent is a molecule responsible for occupying any space of the substrate where the molecule of interest should not be present - passivation. In this case, the blocking agent is supposed to attach everywhere inside the channel except in the gold surfaces where the DNA strands should bind. BSA is prepared from a stock solution of 1 µg/mL which is diluted to a 4% (w/v) working solution with filtered PBS. PAA (8000 [416029] average molecular weight) is diluted from a 45%

(w/w) stock solution to a 4% (w/w) solution also with filtered PBS. For chemiluminescent assays, a Strept-HRP conjugate is diluted from a stock solution to a concentration of 1 mg/mL in PBS and kept at -20ºC. The luminol-based substrate used for the experiments was Luminol SuperSignal®West Femto Chemiluminescent Substrate kit (34094, Thermo Scientific).

MEMS fabrication

As any other device using microfabrication techniques, MEMS are produced in a cleanroom. This is a dedicated room for nano and micromachining with temperature, humidity and light control. It is also equipped with air filtering systems to remove dust and larger microorganisms from the environment. Since there is control over some conditions, the reproducibility of the processes will be increased.

The MEMS used for this work comprise different layers with different purposes. There is a structural layer which corresponds to the part of the device that is responsible for the mechanical motion. Coupled to this layer there is the top electrode, right above the bottom electrode which stands on the substrate. These are the electrodes responsible for actuation of the structure and transduction of the mechanical behaviour. In between both electrodes, there is the sacrificial layer which is removed in the end of the fabrication so that the structure is able to move freely. Finally, another layer of metal is used as ground plane and one made of Au is used for functionalization. A different set of structures was fabricated having various cantilevers composed only by the structural layer and the sacrificial one. The cantilevers had different lengths and the gaps were different for each substarte processed in order to perform a study on stiction.

There is a particular sequence for the fabrication steps that must be followed to obtain a device with the proper characteristics (Figure 9). The first step involves cleaning the substrate with alconox, isopropyl alcohol (IPA) and DI water. The substrate used is corning glass with a thickness of 0.7 mm and an area of 5 x 2.5 cm^2.

The following procedure is the DC-magnetron sputtering deposition of a 150 nm thick layer of TiW. This is the metal used as the bottom electrode. Since the

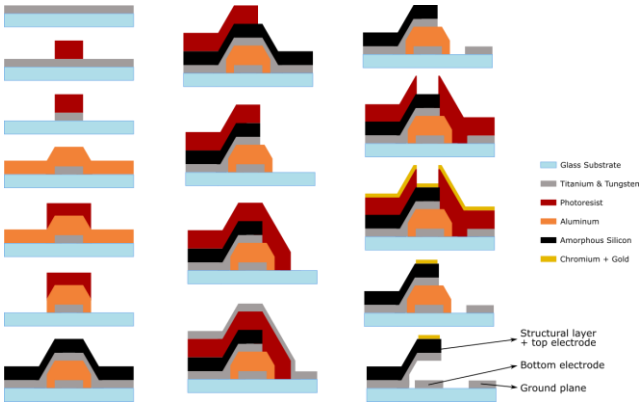

Fig. 9 Schematics of the entire process of MEMS micromachining.

patterning is executed via etching, deposition must be followed by photolithography to define the undesired areas, the areas that have to be etched. All the lithographic steps are performed using a direct write laser (DWL) system and a positive photoresist layer 1.5 µm thick. After developping the photoresist, the sample is ready for the reactive ion etching (RIE) that removes all the areas that are not covered by photoresist. In the end, the photoresist is dissolved in microstrip at room temperature.

Subsequently, the sacrificial layer of aluminum (Al) is deposited by RF-magnetron sputtering. This material is capable of sustaining the high temperatures present during the structural layer deposition and it can be selectivelly etched at the end. The thickness of this layer defines the gap below the structure that in this case was fixed as 1 µm. The deposition is followed by lithography the same way as before, but instead of a dry etch, it is used a wet etch technique to pattern the unprotected regions. For 15 min, the sample is immersed in a commercial Al etchant at room temperature.

The next step corresponds to the deposition of 150 nm TiW for the top electrode and 1 µm of a-Si:H which serves as structural layer. The deposition of the top electrode is similar to the bottom one, while the a-Si:H is deposited using plasma-enhanced chemical vapor deposition (PECVD). Since the patterning of both layers is the same, lithography is only performed after these depositions. After development, they suffer RIE simultaneously.

Afterwards, another lithography takes place to define the pads for wirebonding and the ground plane around the electrical vias. In this case, since the technique used for

metal patterning is lift-off, the lithographic step needs to be done previously to deposition. The material used is again TiW originating a layer with the same thickness as before. After deposition, the photoresist and the undesired metallic parts are removed by lift-off using microstrip.

A layer of Au 50 nm thick is added. Again, because the Au layer is defined via lift-off, first one must do the patterning of the PR using the DWL and only after that the layer of metal is deposited. To improve adhesion of Au onto a-Si:H, a thin layer (10 nm) of chromium (Cr) is deposited in between. Cr is deposited by DC-magnetron sputtering while for Au it is used RF power instead. After the lift-off, the sample is ready for release.

Finally, the wet etch of the sacrificial layer takes place. The Al located in the gap between the bottom and top electrodes is removed and the structure is now free. For the wet etch it is used the same Al etchant as before but now heated at 60ºC to accelerate the process. Then, the sample should be immersed sequentially in DI water, IPA and n-hexane (Sigma-Aldrich). The transition between solutions must be fast to prevent the liquid from drying. The water will wash away the excess of etchant and n-hexane will improve the release of the structures since it creates low surface tension, reducing stiction effects.

Microfluidics fabrication

In paralell, a set of microchannels needs to be produced. The general process is depicted in Figure 10. First a hard mask is produce by deposition of a layer of aluminum in a galss substrate and patterning via wet etch. Then, a silicon substrate is spin-coated with a negative photoresist (SU-8) with the thickness corresponding to the desired height for the microchannels. Aftewards, the hard mask is placed on top of the photoresist and the set is exposed to UV light. After development with PGMEA, the mold is prepared. The material used for the microfluidics is polydimethylsiloxane (PDMS) which is a transparent soft polymer. The mixture of PDMS is poored on top of the mold in a petri dish which is placed in the oven in order to evaporate the solvents and harden (soft lithography). Finally, the PDMS can be easily peeled off and using syringe needles with appropriate dimensions, the inlets and outlets of the channels can be perforated.

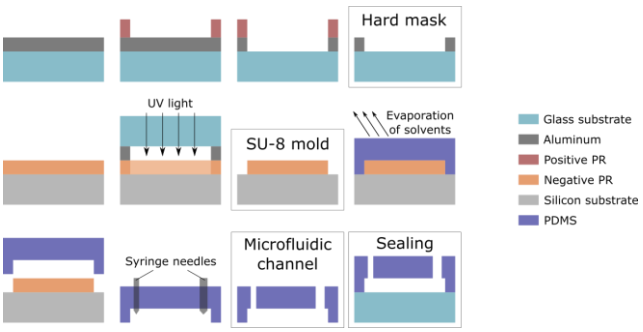

Fig. 10 Schematics of microfluidics fabrication.

The integration with the micromachined chip can be performed using two different techniques: stamping or oxidation. The first one involves spin coatinga a very thin layer with “fresh” PDMS and stamping the pre-fabricated microfluidics structure on this layer. Then, it is aligned with the chip and it goes to oven for solvent evaporation and hardening of the stamped PDMS. The other technique is characterized by an oxidative reaction occuring in a plasma cleaner chamber using oxygen plasma. The plasma creates Si-O groups on both surfaces to be sealed. When they are brought into cont act, Si-O-Si bonds are created.

The fluid handling in microfluidics is made by using syringe pumps connected to the outlets of the microchannels by plastic tubes and metallic plugs. At the inlets, it is placed a micropipette tip with the liquid that is desired to be flowing inside. The liquid flows by differential pressure applied by the pump.

Characterization setups

Before proceeding towards the measurements in the static mode, the resonance frequency was measured for each cantilever. Such method was employed using an optical setup in which a laser is pointed onto the cantilevers beam and the reflected beam is captured by a photodetector. The differences in intensity felt by the photodetector are sent to a spectrum analyzer which extracts the resonance spectrum of the cantilever. In this case, the cantilever is actuated by an AC and a DC voltage. The AC component is directly provided by the spectrum analyzer. In order to determine the resonance frequency and the quality factor, a Lorentz curve is fitted to the data.

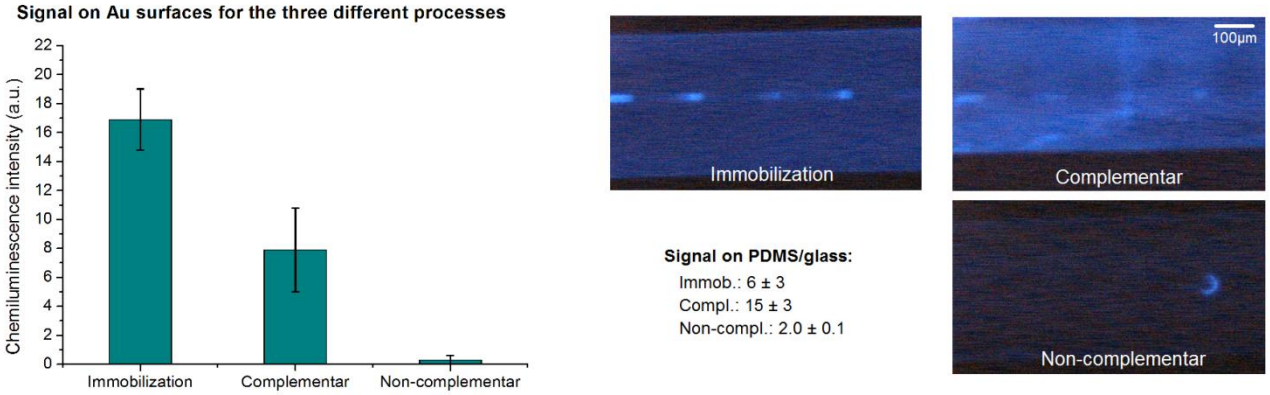

Fig. 11 Results obtained for immobilization and hybridization. (*left*) A plot of the signal on top of Au surfaces is presented along with the (*right*) images captured by chemiluminescence. The bright rectangles correspond to the Au patterns.

Finally, the measurements in the static mode are accomplished by a capacitive readout system. This setup is composed by an LCR meter connected to the PCB where the chip is included by a 4-paired terminal configuration. In between both components it is placed a double multiplexer responsible for switching the measurement for each cantilever. This way it is possible to track various cantilevers sequentially.

4. Results

Biological tests

After optimization of the chemiluminescence assay by varying flow rates, introducing different durations of probe incubation, varying the liquid medium and the blocking agents, it was possible to achieve to a standard protocol for immobilization and hybridization with distinguishable signal on top of gold. Such result is presented in Figure 11 and the protocol used for such purpose is:

Wash w/ IPA	20 µL/min - 3min
Wash w/ TENaCl	20 µL/min - 3min
BSA-4%	0.75 µL/min - 15min
Wash w/ TENaCl	5 µL/min - 1min
Probe	0.1 µL/min - 30min + 3h incub.
Wash w/ TENaCl	5 µL/min - 1min
Target-biotin	0.75 µL/min - 15min
Wash w/ TENaCl	5 µL/min - 1min
Labelling Strept-HRP	1 µL/min - 10min
Wash w/ TENaCl	5 µL/min - 1min
Luminol	20 µL/min

It is clear the difference in intensity of the rectangles composed by gold which show a very bright signal meaning that a lot of probes are attached to the surface. Regarding target recognition, it is found that the oligomers used in this case are highly selective because no distinguishable signal is obtained when using the non-complementar target. This is the desired for any biosensor but especially when it is intended to perform differential measurements between a target molecule and a reference one (non-complementar). Nevertheless, the yield of hybridization seems to be very low when comparing with the signal obtained for immobilization. Anyway, in principle this is not a problem for MEMS sensing.

Unfortunatelly, it was not possible to use fluorescence for tracking the assay because it was observed that gold induces quenching of the fluorophore, eliminating its signal.

Stiction tests

Two different release protocols were applied to the two sets of dies. One of the protocols is the standard release protocol used at INESC-MN comprising a sequential immersion of the die in Al etchant, DI water, IPA and n-hexane. The other one is a simpler procedure using only Al etchant and DI water. The purpose of this comparison was to understand if the additional solutions produce in fact any change in the release and to quantify it. From the optical inspection of the released dies under the microscope, one should obtain the value of the detached length for each cantilever. The two quantities that are allowed to vary are the detachment length and the gap, so if one plots the first as function of the second, a simple fitting procedure to the previously mentioned equation will return the value of work of adhesion for each of the release

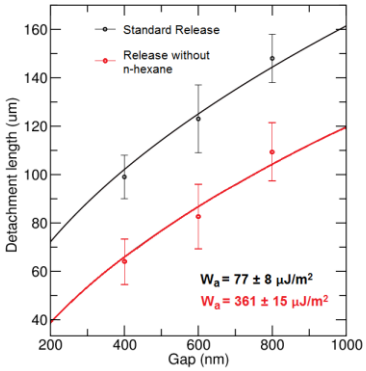

Release protocol	Gap (nm)	l_d (μm)
Standard	400	99 ± 9
	600	123 ± 14
	800	148 ± 10
No n-hexane	400	64 ± 7
	600	78 ± 10
	800	107 ± 9

Fig. 12 Results obtained for the stiction tests. (*left*) Fitting result to extract the values of work of adhesion for each protocol; (*right*) measured detachment lengths.

protocols. In Figure 12 it is represented the resultant fits to the equation of the work of adhesion with the values obtained by this analysis and the measurements used for the procedure.

Because n-hexane is a liquid that creates really low surface tension, the corresponding protocol has a higher detachment length and a lower work of adhesion ($W_a = 77 \pm 8$ μJ/m^2). This means that the forces attracting the beam towards the substrate during release are substantially reduced when the standard protocol is used.

Capacitive measurements

According to the resonance spectrum of the cantilevers, the region around 1.1 MHz corresponds to a non-resonance bandwidth. For that reason, this was the frequency used in the capacitive measurements so that no high-amplitude oscillation is produced.

Unfortunatelly, not much measurements could be perform because a lot of problems with sealing and wire bonding occured to the final devices. Nevertheless, it was possible to define the noise level of the measurements in air and water as 0.04 fF which corresponds to a mechanical deflection of 0.8 nm, way below the tens of nm usually reported for the assays with DNA. It was also possible to sense the staate of flowing and stationary liquid separately as shown in the plots from Figure 13.

5. Conclusions

As first achievement, the present work succeded in quantifying the effects of stiction using the standard protocol at INESC-MN and a simpler one. The standard protocol using n-hexane for reduction in surface tension has an associated binding energy much lower than that of the simple process that finishes using DI water, validating its use. Also, with this tool, it became possible to predict if a cantilever with certain dimensions and material properties is presumed to suffer stiction.

From the biological experiences involving the formation of ssDNA SAM's, an extended study of the effects of the variation of certain conditions on the density of probes immobilized was achieved. Conditions and parameters such as flow rates and duration, incubation, blocking agent and liquid medium were the ones most evaluated. In the end, it was attained a good understanding on the processes involved in SAM's formation and on the tools that help tuning the desired density of probes. Also a protocol for hybridization was established, however, the processes could not be fully-tuned and tested and for that

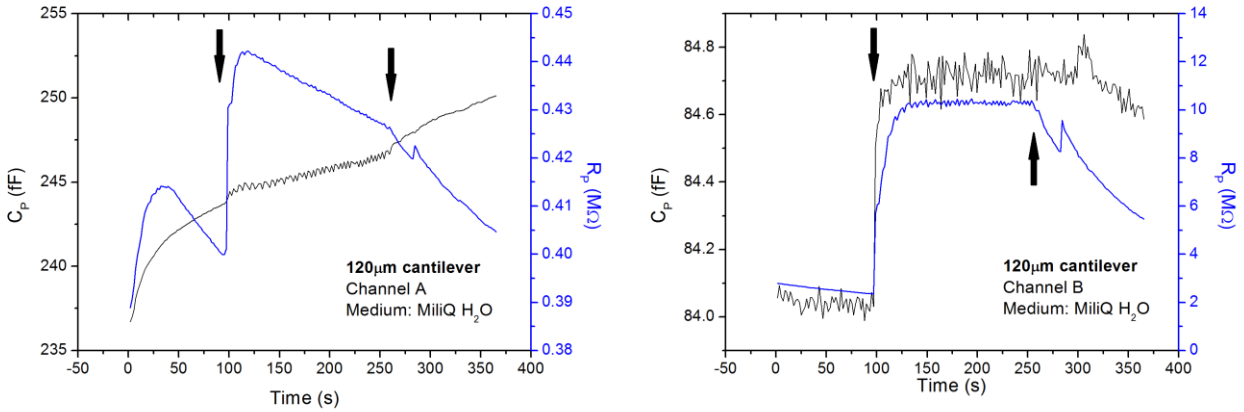

Fig. 13 Results obtained with the capacitive readout setup for two cantilevers with 120μm length placed in two different channels. The black arrows are pointing the instants in which the pump was turned on and off.

reason, only a specific set of conditions and parameters were found to work.

The capacitive measurements on water and air allowed ranking such system with a sensitivity of 0.8 nm of deflection. A complete biological assay could not be completed due to varied problems with the devices, mainly with microfluidics integration, for that reason only some preliminary tests could be performed. However, it was proved that integration of both technologies is feasible.

In a future approach, it would be necessary to study deeper the biological assay, especially hybridization. Further tests on the integrated devices are also relevant but first also a deeper study into sealing methods is advisable because the current strategy does not work with 100% efficiency.

6. Bibliography

[1] S. B. Patil et al. Decoupling competing surface binding kinetics and reconfiguration of receptor footprint for ultrasensitive stress assays. Nature Nanotechnology, 10:899–907, Aug. 2015.

[2] M. Alvarez and L. M. Lechuga. Microcantilever-based platforms as biosensing tools. The Analyst,135:827–836, Jan. 2010.

[3] M. Calleja, P. M. Kosaka, . S. Paulo, and J. Tamayo. Challenges for nanomechanical sensors in biological detection. Nanoscale, 4:4925–4938, June 2012.

[4] J. L. Arlett, E. B. Myers, and M. L. Roukes. Comparative advantages of mechanical biosensors. Nature Nanotechnology, 6:203–215, Mar. 2011.

[5] J. Zhang et al. Rapid and label-free nanomechanical detection of biomarker transcripts in human rna. Nature Nanotechnology, 1:214–220, Nov. 2006.

[6] P. Alpuim, V. Chu, and J. P. Conde. Amorphous and microcrystalline silicon films grown at low temperatures by radio-frequency and hot-wire chemical vapor deposition. Journal of Applied Physics, 86(7):3812–3821, Oct. 1999.

[7] M. Boucinha, P. Brogueira, V. Chu, and J. P. Conde. Amorphous silicon air-gap resonators on large-area substrates. Applied Physics Letters, 77(6):907–909, 2000.

[8] J. Mouro, A. Gualdino, V. Chu, and J. P. Conde. Tunable properties of hydrogenated amorphous / nanocrystalline silicon thin-films for enhanced mems resonators performance. Journal of Microelectromechanical Systems, 23(3):600–609, June 2014.

[9] A. Gualdino, V. Chu, and J. P. Conde. Pressure effects on the dynamic properties of hydrogenated amorphous silicon disk resonators. Journal of Micromechanics and Microengineering, 22(8):85026, Aug. 2012.

[10] J. P. Conde, J. Gaspar, and V. Chu. Low-temperature thin-film silicon mems. Thin Solid Films, 427 (1-2):181–186, Mar. 2003.

[11] J. Gaspar, V. Chu, and J. P. Conde. Electrostatic actuation of thin-film microelectromechanical structures. Journal of Applied Physics, 93(12):10018–10029, Mar. 2003.

[12] A. Gualdino, V. Chu, and J. P. Conde. Study of the out-of-plane vibrational modes in thin-film amorphous silicon micromechanical disk resonators. Journal of Applied Physics, 113(17):174904, Apr. 2013.

[13] Y.-P. Zhao, L. S. Wang, and T. X. Yu. Mechanics of adhesion in mems - a review. Journal of Adhesion Science and Technology, 17(4):519–546, 2003.

[14] E. E. Parker, W. R. Ashurst, C. Carraro, and R. Maboudian. Adhesion characteristics of mems in microfluidic environments. Journal of microelectromechanical systems, 14(5):947–953, Oct. 2005.

[15] R. Maboudian and C. Carraro. Surface chemistry and tribology of mems. Annual Review of Physical Chemistry, 55:35–54, Feb. 2004.

[16] B. Bhushan. Adhesion and stiction: mechanisms, measurement techniques, and methods for reduction. Journal of Vacuum Science and Technology B, 21(6):2262–2296, Nov. 2003.

[17] L. Huang et al. A system based on capacitive interfacing of cmos with post-processed thin-film mems resonators employing synchronous readout for parasitic nulling. Journal of Solid-State Circuits, 50(4):1002–1015, Apr. 2015.

[18] J. Gaspar, V. Chu, and J. P. Conde. Electrostatically actuated thin-film amorphous silicon microbridge resonators. Applied Physics Letters, 97(9):94501, Apr. 2005.

[19] S. B. Patil, A. Guedes, P. P. Freitas, S. Cardoso, V. Chu, and J. P. Conde. On-chip magnetoresistive detection of resonance in microcantilevers. Applied Physics Letters, 95(023502):1–3, July 2009.

[20] M. Li, H. X. Tang, and M. L. Roukes. Ultra-sensitive nems-based cantilevers for sensing, scanned probe and very high-

frequency applications. Nature Nanotechnology, 2(2):114–120, Feb. 2007.

[21] A. Gupta, D. Akin, and R. Bashir. Single virus particle mass detection using microresonators with nanoscale thickness. Applied Physics Letters, 84(11):1976–1978, Mar. 2004.

[22] J. P. Conde, N. Madaboosi, R. Soares, J. Fernandes, P. Novo, G. Moulas, and V. Chu. Lab-on-chip systems for integrated bioanalyses. Essays in Biochemistry, 60:121–131, June 2016.

[23] D. C. Martins, V. Chu, D. Prazeres, and J. P. Conde. Electrical detection of dna immobilization and hybridization by streaming current measurements in microchannels. Applied Physics Letters, 99 (18):183702, Nov. 2011.

[24] M. Boyd-Moss, S. Baratchi, M. D. Venere, and K. Khoshmanesh. Self-contained microfluidic systems: a review. Lab on a Chip, 16:3177–3192, July 2016.

[25] N. Noeth, S. Keller, and A. Boisen. Integrated cantilever-based flow sensors with tunable sensitivity for in-line monitoring of flow fluctuations in microfluidic systems. Sensors, 14:229–244, Jan. 2014.

[26] M. Yue, J. C. Stachowiak, H. Lin, R. Datar, R. Cote, and A. Majumdar. Label-free protein recognition two-dimensional array using nanomechanical sensors. Nano Letters, 8(2):520–524, Jan. 2008.

[27] M. G. von Muhlen, N. D. Brault, S. M. Knudsen, S. Jiang, and S. R. Manalis. Label-free biomarker sensing in undiluted serum with suspended microchannel resonators. Analytical Chemistry, 82(5): 1905–1910, Mar. 2010.

[28] H. Lang, M. Hegner, and C. Gerber. Nanomechanical cantilever array sensors. In D. Bhushan, editor, Handbook of nanotechnology, chapter 15, pages 427–452. Springer, New York, 3rd edition, 2010.

[29] M. F. Hagan, A. Majumdar, and A. K. Chakraborty. Nanomechanical forces generated by surface grafted dna. Journal of Physical Chemistry B, 106(39):10163–10173, Sept. 2002.

[30] A. Sassolas, B. D. Leca-Bouvier, and L. J. Blum. Dna biosensors and microarrays. Chemical Reviews, 108(1):109–139, 2008.

[31] P. M. Kosaka, J. Tamayo, J. J. Ruz, S. Puertas, E. Polo, V. Grazu, J. de la Fuente, and M. Calleja. Tackling reproducibility in microcantilever biosensors: a statistical approach for sensitive and specific end-point detection of immunoreactions. Analyst, 138(3):863–872, Feb. 2013.

[32] J. Fritz. Cantilever biosensors. The Analyst, 133:855–863, Apr. 2008.

[33] K. M. Goeders, J. S. Colton, and L. A. Bottomley. Microcantilevers: sensing chemical interactions via mechanical motion. Chemical Reviews, 108:522–542, Mar. 2008.

[34] R. Shuttleworth. The surface tension of solids. Proceedings of the Physical Society, A63(5):444– 457, May 1950.

[35] G. G. Stoney. The tension of metallic films deposited by electrolysis. Proceedings of the Royal Society of London, A82(553):172–175, May 1909.

[36] A. Boisen, S. Dohn, S. S. Keller, S. Schmid, and M. Tenje. Cantilever-like micromechanical sensors. Reports on Progress in Physics, 74:36101–36131, Feb. 2011.

[37] W. C. Young and R. G. Budynas. Roark's formulas for stress and strain, chapter 8, pages 125–266. McGraw-Hill, New York, 7th edition, 2002.

[38] M. Liangruksa. Effect of surface stress on micromechanical cantilevers for sensing applications. Master's thesis, Virginia Polytechnic Institute and State University, Blacksburg, Virginia, July 2008.

[39] K. L. Ekinci. Electromechanical transducers at the nanoscale: actuation and sensing of motion in nanoelectromechanical systems (nems). Small, 1(8-9):786–797, Aug. 2005.

[40] S. M. Heinrich and I. Dufour. Fundamental theory of resonant mems devices. In O. Brand, I. Dufour, S. M. Heinrich, and F. Josse, editors, Resonant MEMS: fundamentals, implementation, and application, chapter 1, pages 3–28. Wiley, 1st edition, Apr. 2015.

[41] M. Bao. Analysis and design principles of MEMS devices. Elsevier B. V., Amsterdam, 1st edition, 2005.

[42] S. Schmid, L. G. Villanueva, and M. L. Roukes. Fundamentals of nanomechanical resonators, chapter 1-4, pages 1–148. Springer, Switzerland, 2016.

[43] M. Lalanne, P. Berthier, and J. D. Hagopian. Mechanical vibrations for engineers, chapter 1, pages 1–36. John Wiley and Sonsl, New York, 1984.

[44] M. I. Younis. MEMS linear and nonlinear statics and dynamics, chapter 1-4, pages 1–154. Springer, New York, 2011.

[45] B. Bahreyni. Fabrication and design of resonant microdevices. series 3. William Andrew, New York, 2008.

[46] R. Marathe. Active sensing in silicon-based MEMS resonators. Phd thesis, Massachusetts Institute of Technology, June 2015.

[47] G. J. O'Brien, D. J. Monk, and L. Lin. Mems cantilever beam electrostatic pull-in model. In P. D. Franzon, A. P. Malshe, and F. E. Tay, editors, Design, characterization, and packaging for MEMS and microelectronics II, volume 4593, pages 1–4, Nov. 2001.

[48] P. Kumar, R. Elavarasi, P. B. Eladi, and M. Gopikrishnan. Pull-in voltage study of various structured cantilever and fixed-fixed beam models using comsol multiphysics. Indian Journal of Science and Technology, 8(14):1–9, July 2015.

[49] Y. Huang, H. Chen, and W. Hsu. An analytical model for calculating the pull-in voltage of micro cantilever beams subjected to tilted and curled effects. Microelectronic Engineering, 125:73–77, Jan. 2014.

[50] C. H. Mastrangelo and C. H. Hsu. Mechanical stability and adhesion of microstructures under capillary forces - part i: basic theory. Journal of Microelectromechanical systems, 2(1):33–43, Mar. 1993.

[51] C. H. Mastrangelo and C. H. Hsu. Mechanical stability and adhesion of microstructures under capillary forces - part ii: experiments. Journal of Microelectromechanical systems, 2(1):44–55, Mar. 1993.

[52] M. R. Houston, R. T. Howe, and R. Maboudian. Effect of hydrogen termination on the work of adhesion between rough polycrystalline silicon surfaces. Journal of Applied Physics, 81(8):3474– 3483, Apr. 1997.

[53] P. Tabeling. Introduction to microfluidics. Oxford University Press, Oxford, Nov. 2005.

[54] B. E. Rapp. Microfluidics: modeling, mechanics, and mathematics, chapter 9-24, pages 241–494. Micro and nano technologies. William Andrew - Elsevier, Oxford, 2017.

[55] R. Pedersen, A. N. Marchi, J. Majikes, J. A. Nash, N. A. Estrich, D. S. Courson, C. K. Hall, S. L. Craig, and T. H. LaBean. Handbook of nanomaterials properties, chapter 34, pages 1125–1157. Springer, Berlin, 1st edition, 2014.

[56] J. Watson, T. Baker, S. Bell, A. Gann, M. Levine, and R. Losick. Molecular biology of the gene, chapter 6, pages 1–33. Cold Spring Harbor Laboratory Press, New York, 5th edition, 2004.

[57] T. F. Scientific. Fluorescence fundamentals, accessed on 29th Jun 2017. https://www.thermofisher.com/pt/en/home/references/molecular-probes-thehandbook/ introduction-to-fluorescence-techniques.html.

[58] C. Caneira. Bead-based microfluidic system for dna/rna detection. Master's thesis, Instituto Superior Técnico, Lisboa, Nov. 2015.

[59] T. F. Scientific. Chemiluminescent western blotting, accessed on 29th Jun 2017. https://www.thermofisher.com/pt/en/home/life-science/protein-biology/protein-biology-learningcenter/

protein-biology-resource-library/pierce-protein-methods/chemiluminescent-westernblotting. html.

[60] A. W. Peterson, R. J. Heaton, and R. M. Georgiadis. The effect of surface probe density on dna hybridization. Nucleic Acids Research, 29(24):5163–5168, Oct. 2001.